Mimicking graphene with polaritonic spin vortices

Dmitry R. Gulevich* and Dmitry Yudin
ITMO University, St. Petersburg 197101, Russia

(Received 28 July 2017; revised manuscript received 4 September 2017; published 18 September 2017)

Exploring the properties of strongly correlated systems through quantum simulation with photons, cold atoms, or polaritons represents an active area of research. In fact, the latter sheds light on the behavior of complex systems that are difficult to address in the laboratory or to tackle numerically. In this study, we discuss an analog of graphene formed by exciton-polariton spin vortices arranged into a hexagonal lattice. We show how graphene-type dispersion at different energy scales arises for several types of exciton-polariton spin vortices. In contrast to previous studies of exciton polaritons in artificial lattices, the use of exciton-polariton spin vortex modes offers a richer playground for quantum simulations. In particular, we demonstrate that the sign of the nearest-neighbor coupling strength can be inverted.

DOI: 10.1103/PhysRevB.96.115433

I. INTRODUCTION

Investigation of low-dimensional strongly correlated electron systems remains one of the most exciting fields of modern condensed-matter physics. Nevertheless, only a limited number of physically relevant problems can be solved in a closed analytical form. However, some meaningful information about the nature of ground states and correlation functions can be gained by making use of quantum simulators—systems that, while being different physical systems, are described by the same or similar equations on the mathematical level. Of particular importance and interest are quantum simulators based on exciton polaritons, a quasiparticle emerging from the strong light-matter coupling that simultaneously inherits properties from both excitons and photons. Exciton polaritons can be confined in artificially fabricated lattices and thus used to model the properties of crystalline solids.

Exploring typical features of exciton polaritons confined within two-dimensional lattices represents an active area of research. In fact, in just the past few years, the properties of a polaritonic honeycomb lattice [1–7], a benzene molecule [8], a kagome lattice [9,10], and a Lieb [11] lattice were addressed theoretically and experimentally, and the emergence of nontrivial topological phases of exciton polaritons was discussed [12–16]. The use of exciton polaritons allows us to study condensed-matter phenomena in a well-controllable environment where the parameters of the systems can be changed by varying the confining potential landscape, changing the effective mass of a polariton, the frequency of excitations, and the separation between lattice sites. In this paper, we show that the sign of the coupling strength J can also be controlled by involving higher excited states of the p band in the form of polaritonic spin vortices.

As was first shown by Abrikosov [17], when a magnetic field is present it penetrates the superconducting condensate forming a triangular lattice of vortices. Each vortex carries a magnetic flux, and its core represents a nonsuperconducting phase. The formation of vortices has also been shown to take place in Bose-Einstein condensates (BECs) of ultracold quantum atoms [18–20] and exciton polaritons [21,22]. The formalism developed for vortex matter in superconductors can be easily generalized to magnetic skyrmion systems [23]. Skyrmions are characterized by a quantized topological winding number, and they are known to condense in a lattice quite similar to an Abrikosov vortex lattice in superconductors [24–26].

The first experimental observation of vortices in exciton-polariton systems in the regime of stationary incoherent pumping was reported in Ref. [21]. Interestingly, in contrast to BECs of ultracold atoms, the formation of vortices of exciton polaritons is associated with the presence of disorder in any realistic semiconductor heterostructure, and the nonequilibrium nature of the condensate. The optimal geometry of a vortex lattice is purely determined by the confining potential landscape in which polariton liquid is trapped. One more possibility to excite exciton-polariton vortices is using a light beam with properly adjusted angular momentum [22]. In the field of a confining potential, the exciton-polariton liquid is no longer uniform, but at $T = 0$ it can be described by the spinor analog of the Gross-Pitaevskii equation for the wave function of a condensate. Solutions to this equation are known to describe many phenomena, ranging from simple equilibrium configurations to highly inhomogeneous vortices and bright and dark solitons [27].

II. POLARITONIC SPIN VORTICES

Recently, the use of tunable open-access microcavities (OAMs) [28,29] led to the observation of spin textures of exciton polaritons—polaritonic spin vortices (PSVs). This became possible due to a large TE-TM splitting observed in OAMs, which is reported to exceed those in monolithic cavities by a factor of 3 [29]. The TE-TM splitting of exciton-polariton systems arises mainly due to the photonic component. The polarization splitting of exciton polaritons results from the polarization-dependent reflection off dielectric mirrors in microcavity resonators [30], which manifests itself in the difference between the dispersion relations for polaritons polarized longitudinally and transversely to the direction of propagation (a similar, yet more delicate, effect also arises due to the excitonic component [31]). In the effective-mass approximation, the TE-TM splitting can be described by two masses m_{TM} and m_{TE} for polaritons polarized longitudinally

*d.r.gulevich@metalab.ifmo.ru

(TM mode) or transversely (TE mode) with respect to the in-plane wave vector and in direct correspondence with the TE/TM resonator modes. The TE-TM splitting in polariton systems leads to the emergence of the effective spin-orbit interaction [8,32,33], which has been recently exploited in various settings related to topological properties of exciton polaritons [5,9,13,34].

Exciton polaritons confined to a patterned structure with the potential energy landscape $V(x,y)$, and neglecting polariton-polariton interactions, are described by a system of coupled spinor Schrödinger equations [29,35,36],

$$\begin{aligned} i\frac{\partial\psi_+}{\partial t} &= -\Delta\psi_+ + V(x,y)\,\psi_+ + \beta(\partial_x - i\partial_y)^2\psi_-, \\ i\frac{\partial\psi_-}{\partial t} &= -\Delta\psi_- + V(x,y)\,\psi_- + \beta(\partial_x + i\partial_y)^2\psi_+, \end{aligned} \tag{1}$$

where $\psi_\pm = (\psi_x \mp i\psi_y)/\sqrt{2}$ are two circular polarization components forming a spinor $\psi = \psi_+\hat{e}_+ + \psi_-\hat{e}_-$, with the basis vectors given by $\hat{e}_\pm = (\hat{e}_x \pm i\hat{e}_y)/\sqrt{2}$, and β is a parameter that corresponds to the TE-TM splitting [37]. Here and in what follows, we work with normalized units by introducing a characteristic length L of the potential profile and related to it the unit energy $E_0 = \hbar^2/(2m^*L^2)$, on the condition that $m^* = 2m_{\mathrm{TE}}m_{\mathrm{TM}}/(m_{\mathrm{TE}} + m_{\mathrm{TM}})$ is the effective mass of a polariton. In the normalized units, the TE-TM splitting parameter $\beta = (m_{\mathrm{TE}}^{-1} - m_{\mathrm{TM}}^{-1})m^*/2$. Note that the sign of β can be both positive and negative depending on the offset of the frequency from the center of the stop band of the distributed Bragg reflector [30].

In a typical experimental setup [29] used to observe PSVs, the top concave mirror induces a strong and almost harmonic lateral confinement of polaritons. Thus, mathematically, PSVs represent stationary solutions of Eq. (1) in the presence of the potential $V(x,y) = x^2 + y^2$. Substituting the ansatz

$$\psi_\pm(r,\varphi) = e^{-i\mu t + i(n\mp1)\varphi} f_\pm(r), \tag{2}$$

where r is the radial distance, into Eq. (1) [compare (2) to solutions in a quasi-1D ring [34]] yields the equation on the amplitudes $f_\pm(r)$,

$$\begin{aligned} \mu f_\pm = &\left[-\partial_r^2 - \frac{1}{r}\partial_r + \frac{(n\mp1)^2}{r^2} + V(r)\right] f_\pm \\ &+ \beta\left[\partial_r^2 + \frac{(1\pm2n)}{r}\partial_r + \frac{n^2-1}{r^2}\right] f_\mp. \end{aligned} \tag{3}$$

With the requirement that the amplitudes $f_\pm(r)$ behave regularly at $r = 0$ and take zero value at infinity, $f(\infty) \to 0$, we obtain the spectrum by solving numerically the eigenvalue problem (3). As seen from Fig. 1(a), if we take $\beta = 0$, the spectrum coincides with that of Laguerre-Gauss modes. In the presence of a nonzero β, the degeneracy is lifted and the spectrum is split into individual modes. The spectrum is symmetric with respect to changing sign of β, although the spin texture is not: two different types of spin textures are possible at the same energy when β changes its sign. The amplitudes $f_\pm(r)$ of the first few lowest-energy PSVs are shown in Figs. 1(b)–1(d) at a chosen value of TE-TM splitting, $\beta = -0.2$. It is clearly visible that $|f_+(r)| = |f_-(r)|$ for the two $n = 0$ vortices, which are, therefore, linearly polarized.

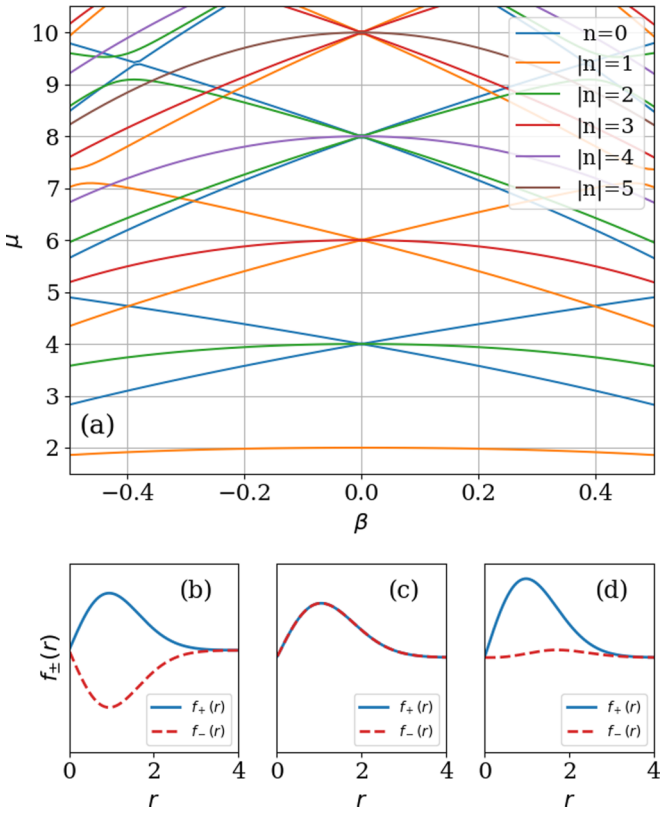

FIG. 1. (a) Energy spectrum of polaritonic spin vortices in the harmonic potential given by the eigenvalue problem (3). Profiles of the lowest-energy spin vortices, depicted for TE-TM splitting $\beta = -0.2$, are shown in panels (b), (c), and (d). Panels (b) and (c) correspond to the two lowest-energy states with $n = 0$, $\mu = 3.58$, and $\mu = 4.38$, and (c) to the lowest-energy state with $n = 2$ and $\mu = 3.93$.

Introducing a linear polarization basis defined by $\psi_x = (\psi_+ + \psi_-)/\sqrt{2}$, $\psi_y = i(\psi_+ - \psi_-)/\sqrt{2}$, one can distinctly notice that the vortex in Fig. 1(b) is polarized along the azimuthal direction, and the vortex in Fig. 1(c) is polarized along the radial direction (cf. Ref. [29]).

III. POLARITONIC SPIN VORTEX GRAPHENE

While the technology of fabricating an artificial lattice of a solid-state microcavity seems to be well developed and actively applied to the creation of exciton polaritons analogs of condensed-matter systems [38], the coupling of multiple OAMs into an array has yet to be achieved. The dependence of the coupling strength of two OAMs on its separation has recently been studied in Ref. [39].

A system of coupled OAMs arranged into an artificial lattice can be described by the system (1) with the potential landscape

$$V(x,y) = V_0 \min_{i\in\Omega}\left[1, \frac{(x-x_i)^2 + (y-y_i)^2}{R^2}\right], \tag{4}$$

where R is the radius of a single OAM, and the minimum is taken over the set Ω of individual OAMs. To investigate the emergent behavior of PSVs in lattices, we focus on a honeycomb lattice. In our numerical calculation of the band structure, we use model (4) with the cavity diameter matching the cavity separation (i.e., the touching cavities, which is an

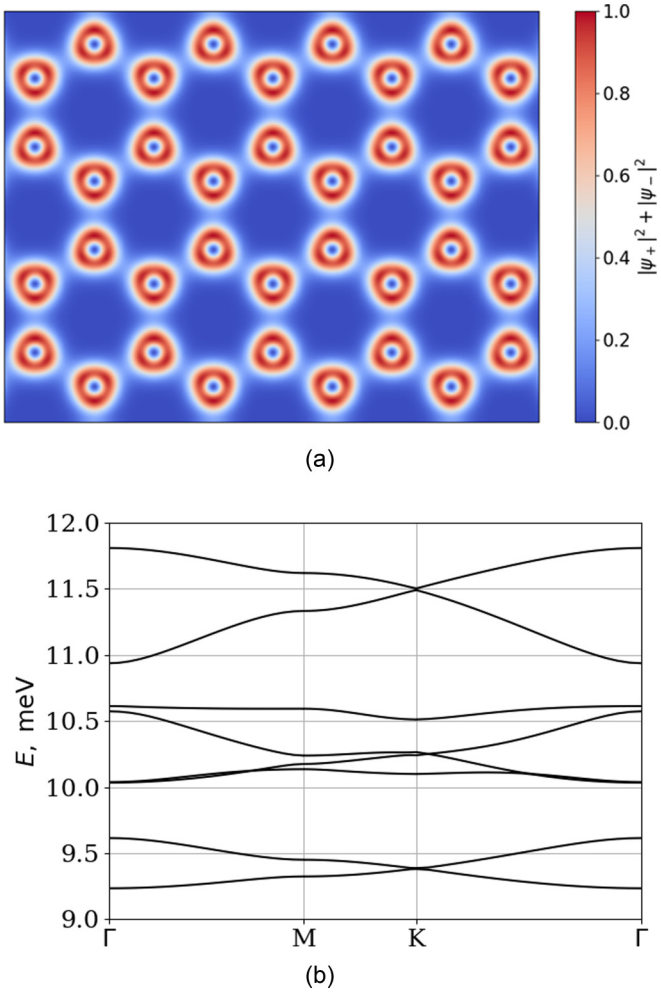

FIG. 2. (a) Numerically calculated Bloch state of polaritonic spin vortex graphene at $k_x = k_y = 0$. The color scale represents the numerically calculated spatial distribution of the exciton polariton density (arbitrary units) at $\beta = -0.2$. (b) Graphenelike dispersion formed by the lowest polaritonic spin vortices. Panels (a) and (b) are the results of our numerical calculations with a 2D model (1) and potential (4) in the form of a honeycomb lattice. Parameters $m^* = 2 \times 10^{-5} m_e$, $\beta = -0.2$, cavity diameter 4 μm, and potential strength $V_0 = 15$ meV were used in the calculation.

intermediate regime of coupling in the experimental study [39]), and parameters $m^* = 2 \times 10^{-5} m_e$, $\beta = -0.2$, cavity diameter 4 μm, and potential strength $V_0 = 15$ meV, which are realistic for polaritonic systems. A typical density distribution in a Bloch vector formed by the lowest-energy PSV [the one presented in Fig. 1(b)] is shown in Fig. 2(a). The complete p band of the calculated band structure is shown in Fig. 2. Therein, graphenelike dispersions are seen, arising due to each of the three types of PSVs. Nearly perfect graphene dispersion with well-visible Dirac cones at the top and bottom of the p band in Fig. 2 is produced by the lower (in energy) and the upper $n = 0$ vortices [Figs. 1(b) and 1(c)]. The intermediate energies in Fig. 2 are occupied by the bands of the two $n = \pm 2$ vortices, which are a doubly degenerate state in an isolated harmonic well. The finite intercavity coupling lifts the degeneracy and makes the band diagram more intricate than that of the $n = 0$ vortices.

In contrast to previous studies of exciton polaritons in artificial lattices, the use of exciton-polariton spin vortex modes offers a novel platform for emulating solid-state systems, i.e., the inverted sign of the nearest-neighbor coupling strength. Indeed, in the conventional implementation of artificial lattices with exciton polaritons, the coupling strength has been shown to be controlled by changing the landscape of the potential and separation between individual microcavity pillars or OAMs. However, the sign of the coupling parameter J in the tight-binding Hamiltonian $\hat{H} = -J \sum_{\langle ij \rangle} (\hat{a}_i^\dagger \hat{a}_j + \text{H.c.})$ remains always positive for the s-band modes involved (it favors the neighboring sites to match their wave-function phases). Using PSVs as a building block of artificial lattice systems, it is possible to achieve the opposite limit of negative coupling strength, $J < 0$. Therefore, PSVs provide further control over polaritonic systems and their application in modeling condensed-matter phenomena.

IV. OTHER TYPES OF POLARITONIC SPIN VORTEX LATTICES

Apart from the honeycomb lattice, it is instructive to look at the novel features brought about by the use of PSVs as fundamental modes of artificial lattices, such as a kagome lattice and a square lattice.

The kagome lattice [40] is characterized by a high degree of frustration and three nonequivalent sites per unit cell. It has been attracting a great deal of interest in relation to the topological properties of magnetic systems [41,42] and, very recently, exciton polaritons [9,10,43]. In the tight-binding approximation with nearest-neighbor coupling, the highest-energy band of a polaritonic kagome lattice is completely flat. Arranging PSVs into a kagome lattice allows us to obtain the negative sign of the nearest-neighbor coupling, which results in the flatband being the lowest-energy state of the whole p band.

With periodically arranged PSVs, it is possible to deliver an analogy with magnetic systems. At $\beta < 0$, the distribution of the electric field in the lowest-energy PSV is strictly azimuthal (it is perpendicular to the radial direction and oscillates between clockwise and anticlockwise directions with polariton frequency). According to the Maxwell equations, such a configuration of the electric field is associated with a magnetic field at the center of the vortex, which is transverse to the microcavity plane and oscillating between the up or down directions. Because two neighboring PSVs favor opposite phases, the oscillating magnetic-field vectors in the neighboring sites prefer the opposite orientation, i.e., antiferromagnetic ordering. Indeed, if PSVs are arranged into a square lattice with lattice spacing a, the energy minimum of the PSV configuration is achieved at the corners of the first Brillouin zone $k_x = k_y = \pm \pi/a$, in direct analogy with the antiferromagnetic arrangement of real magnetic moments.

V. CONCLUSIONS

We have demonstrated an analog of graphene based on PSVs. A well-recognizable graphene dispersion arises for several types of PSVs at different energy scales. Due to the nonequilibrium nature of exciton polaritons, either of the dispersions can be observed by tuning the excitation

frequency of the polariton system. With realistic parameters $m^* = 2 \times 10^{-5} m_e$ and $\beta = -0.2$, cavity diameter 4 μm, and potential strength $V_0 = 15$ meV, we obtained a two-graphene dispersion band separation exceeding 500 μeV at the Γ point, which can in principle be observed experimentally. Finally, to ensure that the effective-mass approximation used in model (1) is valid at the energies of the PSV bands, one can either choose to work in the regime of strong negative detuning between the exciton and photon branches, or use materials with large Rabi splitting [44,45].

We have also shown that the sign of the coupling strength J in polaritonic systems can be effectively controlled by employing PSVs. In the case of a kagome lattice, the negative coupling strength J causes the usual kagome band structure to appear upside down, i.e., the flatband is the lowest energy of the whole p band. This is highly favorable for observation of exciton-polariton condensation, and, in principle, it may be exploited for engineering of the polaritonic analog of the quantum Hall effect.

ACKNOWLEDGMENTS

We acknowledge the support from the Russian Science Foundation under the Project 17-12-01359.

[1] T. Jacqmin, I. Carusotto, I. Sagnes, M. Abbarchi, D. D. Solnyshkov, G. Malpuech, E. Galopin, A. Lemaître, J. Bloch, and A. Amo, Phys. Rev. Lett. **112**, 116402 (2014).
[2] K. Kusudo, N. Y. Kim, A. Löffler, S. Höfling, A. Forchel, and Y. Yamamoto, Phys. Rev. B **87**, 214503 (2013).
[3] M. Milićević, T. Ozawa, P. Andreakou, I. Carusotto, T. Jacqmin, E. Galopin, A. Lemaître, L. Le Gratiet, I. Sagnes, J. Bloch, and A. Amo, 2D Mater. **2**, 034012 (2015).
[4] A. V. Nalitov, G. Malpuech, H. Terças, and D. D. Solnyshkov, Phys. Rev. Lett. **114**, 026803 (2015).
[5] A. V. Nalitov, D. D. Solnyshkov, and G. Malpuech, Phys. Rev. Lett. **114**, 116401 (2015).
[6] O. Bleu, D. D. Solnyshkov, and G. Malpuech, Phys. Rev. B **95**, 115415 (2017).
[7] O. Bleu, D. D. Solnyshkov, and G. Malpuech, Phys. Rev. B **95**, 235431 (2017).
[8] V. G. Sala, D. D. Solnyshkov, I. Carusotto, T. Jacqmin, A. Lemaître, H. Terças, A. Nalitov, M. Abbarchi, E. Galopin, I. Sagnes, J. Bloch, G. Malpuech, and A. Amo, Phys. Rev. X **5**, 011034 (2015).
[9] D. R. Gulevich, D. Yudin, I. V. Iorsh, and I. A. Shelykh, Phys. Rev. B **94**, 115437 (2016).
[10] D. R. Gulevich, D. Yudin, D. V. Skryabin, I. V. Iorsh, and I. A. Shelykh, Sci. Rep. **7**, 1780 (2017).
[11] C. E. Whittaker, E. Cancellieri, P. M. Walker, D. R. Gulevich, H. Schomerus, D. Vaitiekus, B. Royall, D. M. Whittaker, E. Clarke, I. V. Iorsh, I. A. Shelykh, M. S. Skolnick, and D. N. Krizhanovskii, arXiv:1705.03006.
[12] T. Karzig, C.-E. Bardyn, N. H. Lindner, and G. Refael, Phys. Rev. X **5**, 031001 (2015).
[13] C.-E. Bardyn, T. Karzig, G. Refael, and T. C. H. Liew, Phys. Rev. B **91**, 161413 (2015).
[14] K. Yi and T. Karzig, Phys. Rev. B **93**, 104303 (2016).
[15] S. M. de Vasconcellos, A. Calvar, A. Dousse, J. Suffczyński, N. Dupuis, A. Lemaître, I. Sagnes, J. Bloch, P. Voisin, and P. Senellart, Appl. Phys. Lett. **99**, 101103 (2011).
[16] D. D. Solnyshkov, A. V. Nalitov, and G. Malpuech, Phys. Rev. Lett. **116**, 046402 (2016).
[17] A. A. Abrikosov, J. Phys. Chem. Solids **2**, 199 (1957).
[18] K. W. Madison, F. Chevy, W. Wohlleben, and J. Dalibard, Phys. Rev. Lett. **84**, 806 (2000).
[19] J. R. Abo-Shaeer, C. Raman, J. M. Vogels, and W. Ketterle, Science **292**, 476 (2001).
[20] I. Bloch, J. Dalibard, and W. Zwerger, Rev. Mod. Phys. **80**, 885 (2008).
[21] K. G. Lagoudakis, M. Wouters, M. Richard, A. Baas, I. Carusotto, R. André, L. S. Dang, and B. Deveaud-Pledran, Nat. Phys. **4**, 706 (2008).
[22] D. Sanvitto, F. M. Marchetti, M. H. Szymanska, G. Tosi, M. Baudisch, F. P. Laussy, D. N. Krizhanovskii, M. S. Skolnick, L. Marrucci, A. Lemaitre, J. Bloch, C. Tejedor, and L. Vina, Nat. Phys. **6**, 527 (2010).
[23] A. N. Bogdanov and D. A. Yablonskii, Sov. Phys. JETP **68**, 101 (1989).
[24] S. Mühlbauer, B. Binz, F. Jonietz, C. Pfleiderer, A. Rosch, A. Neubauer, R. Georgii, and P. Böni, Science **323**, 915 (2009).
[25] X. Z. Yu, Y. Onose, N. Kanazawa, J. H. Park, J. H. Han, Y. Matsui, and Y. Nagaosa, Nature (London) **465**, 901 (2010).
[26] J. H. Han, J. Zang, Z. Yang, J.-H. Park, and N. Nagaosa, Phys. Rev. B **82**, 094429 (2010).
[27] A. Aftalion, *Vortices in Bose-Einstein Condensates* (Birkhäuser, Secaucus, NJ, 2006).
[28] S. Dufferwiel *et al.*, Appl. Phys. Lett. **104**, 192107 (2014).
[29] S. Dufferwiel *et al.*, Phys. Rev. Lett. **115**, 246401 (2015).
[30] G. Panzarini, L. C. Andreani, A. Armitage, D. Baxter, M. S. Skolnick, V. N. Astratov, J. S. Roberts, A. V. Kavokin, M. R. Vladimirova, and M. A. Kaliteevski, Phys. Rev. B **59**, 5082 (1999).
[31] M. Z. Maialle, E. A. de Andrada e Silva, and L. J. Sham, Phys. Rev. B **47**, 15776 (1993).
[32] A. Kavokin, G. Malpuech, and M. Glazov, Phys. Rev. Lett. **95**, 136601 (2005).
[33] C. Leyder, M. Romanelli, J. Ph. Karr, E. Giacobino, T. C. H. Liew, M. M. Glazov, A. V. Kavokin, G. Malpuech, and A. Bramati, Nat. Phys. **3**, 628 (2007).
[34] D. R. Gulevich, D. V. Skryabin, A. P. Alodjants, and I. A. Shelykh, Phys. Rev. B **94**, 115407 (2016).
[35] H. Flayac, I. A. Shelykh, D. D. Solnyshkov, and G. Malpuech, Phys. Rev. B **81**, 045318 (2010).
[36] M. Toledo-Solano, M. E. Mora-Ramos, A. Figueroa, and Y. G. Rubo, Phys. Rev. B **89**, 035308 (2014).
[37] Our definition of parameter β differs from Refs. [4,5,16,35] but is consistent with the theoretical and experimental works in Refs. [29,36].
[38] C. Schneider, K. Winkler, M. D. Fraser, M. Kamp, Y. Yamamoto, E. A. Ostrovskaya, and S. Höfling, Rep. Prog. Phys. **80**, 016503 (2017).

[39] S. Dufferwiel *et al.*, Appl. Phys. Lett. **107**, 201106 (2015).
[40] M. Mekata, Phys. Today **56**(2), 12 (2003).
[41] M. Pereiro, D. Yudin, J. Chico, C. Etz, O. Eriksson, and A. Bergman, Nat. Commun. **5**, 4815 (2014).
[42] R. Chisnell, J. S. Helton, D. E. Freedman, D. K. Singh, R. I. Bewley, D. G. Nocera, and Y. S. Lee, Phys. Rev. Lett. **115**, 147201 (2015).
[43] N. Masumoto, N. Y. Kim, T. Byrnes, K. Kusudo, A. Löffler, S. Höfling, A. Forchel, and Y. Yamamoto, New J. Phys. **14**, 065002 (2012).
[44] S. Faure, T. Guillet, P. Lefebvre, T. Bretagnon, and B. Gil, Phys. Rev. B **78**, 235323 (2008).
[45] K. Li, W. Wang, Z. Chen, N. Gao, W. Yang, W. Li, H. Chen, S. Li, H. Li, P. Jin, and J. Kang, Sci. Rep. **3**, 3551 (2013).